# Implications of Noise and Neural Heterogeneity for Vestibulo-Ocular Reflex Fidelity

**Timothy M. Hospedales**
*t.hospedales@ed.ac.uk*
**Mark C. W. van Rossum**
*mvanross@ed.ac.uk*
*Institute for Adaptive and Neural Computation, School of Informatics, University of Edinburgh, Edinburgh EH1 2QL, U.K.*

**Bruce P. Graham**
*b.graham@ed.ac.uk*
*Department of Computing Science and Mathematics, University of Stirling, Stirling FK9 4LA, U.K.*

**Mayank B. Dutia**
*m.b.dutia@ed.ac.uk*
*Centre for Integrative Physiology, School of Biomedical Sciences, University of Edinburgh, Edinburgh EH8 9XD, U.K.*

**The vestibulo-ocular reflex (VOR) is characterized by a short-latency, high-fidelity eye movement response to head rotations at frequencies up to 20 Hz. Electrophysiological studies of medial vestibular nucleus (MVN) neurons, however, show that their response to sinusoidal currents above 10 to 12 Hz is highly nonlinear and distorted by aliasing for all but very small current amplitudes. How can this system function in vivo when single cell response cannot explain its operation? Here we show that the necessary wide VOR frequency response may be achieved not by firing rate encoding of head velocity in single neurons, but in the integrated population response of asynchronously firing, intrinsically active neurons. Diffusive synaptic noise and the pacemaker-driven, intrinsic firing of MVN cells synergistically maintain asynchronous, spontaneous spiking in a population of model MVN neurons over a wide range of input signal amplitudes and frequencies. Response fidelity is further improved by a reciprocal inhibitory link between two MVN populations, mimicking the vestibular commissural system in vivo, but only if asynchrony is maintained by noise and pacemaker inputs. These results provide a previously missing explanation for the full range of VOR function and a novel account of the role of the intrinsic pacemaker conductances in MVN cells. The values of diffusive noise and pacemaker currents that give optimal response fidelity yield firing statistics similar**

**to those in vivo, suggesting that the in vivo network is tuned to optimal performance. While theoretical studies have argued that noise and population heterogeneity can improve coding, to our knowledge this is the first evidence indicating that these parameters are indeed tuned to optimize coding fidelity in a neural control system in vivo.**

## 1 Introduction

A number of recent analytical and computational modeling studies have considered the signal processing characteristics of neuronal populations and the effects of spontaneous spiking activity on the population response (Knight, 1972; Gerstner, 2000; van Rossum, Turrigiano, & Nelson, 2002; Masuda & Aihara, 2003; Masuda, Doiron, Longtin, & Aihara, 2005). These studies have revealed that the population response of a set of tonically active, asynchronously firing neurons can encode a common input signal with high fidelity and linearity over a wide operating range. Moreover, the population response to changes in synaptic input is virtually immediate, since at any given time, there is always a subset of neurons that are near firing threshold. This contrasts with the population response of neurons lacking tonic spiking activity, where changes in input will either evoke no response if they are too small or generate a response with a certain integration latency and a tendency toward synchronicity and periodicity over a relatively restricted linear range (e.g., Diesman, Gewaltig, & Aertsen, 1999). However, the question as to which of these codes are used in sensory systems is difficult to address in pathways that have extensive downstream processing, which could extract different aspects of the activity. Therefore, we researched this issue in a relatively simple system, the brainstem horizontal vestibulo-ocular reflex (hVOR) pathway (see Figure 1), which routes sensory input almost directly to the motor output without any subsequent processing.

The hVOR pathway has been extensively investigated experimentally (Huterer & Cullen, 2002; Minor, Lasker, Backous, & Hullar, 1999; Ramachandran & Lisberger, 2005, 2006), and many analytical and cellular models exist (Cartwright & Curthoys, 1996; Arnold & Robinson, 1997; Graham & Dutia, 2001; Cartwright, Curthoys, & Gilchrist, 1999; Cartwright, Gilchrist, Burgess, & Curthoys, 2003). Neurons in the medial vestibular nucleus (MVN; type I neurons, see Figure 1) play a key role in transforming head velocity inputs from horizontal semicircular canal afferents into motor commands to the abducens and oculomotor nuclei, which generate compensatory eye movements and stabilize gaze. The MVNs of the two sides are linked by a reciprocal inhibitory commissural pathway involving type II inhibitory interneurons (see Figure 1), which is essential for the normal gain and time constant of the hVOR. While additional pathways, including the cerebellar flocculus, are necessary for gain calibration and adaptive control of the VOR, the essential circuitry in Figure 1 represents the core VOR
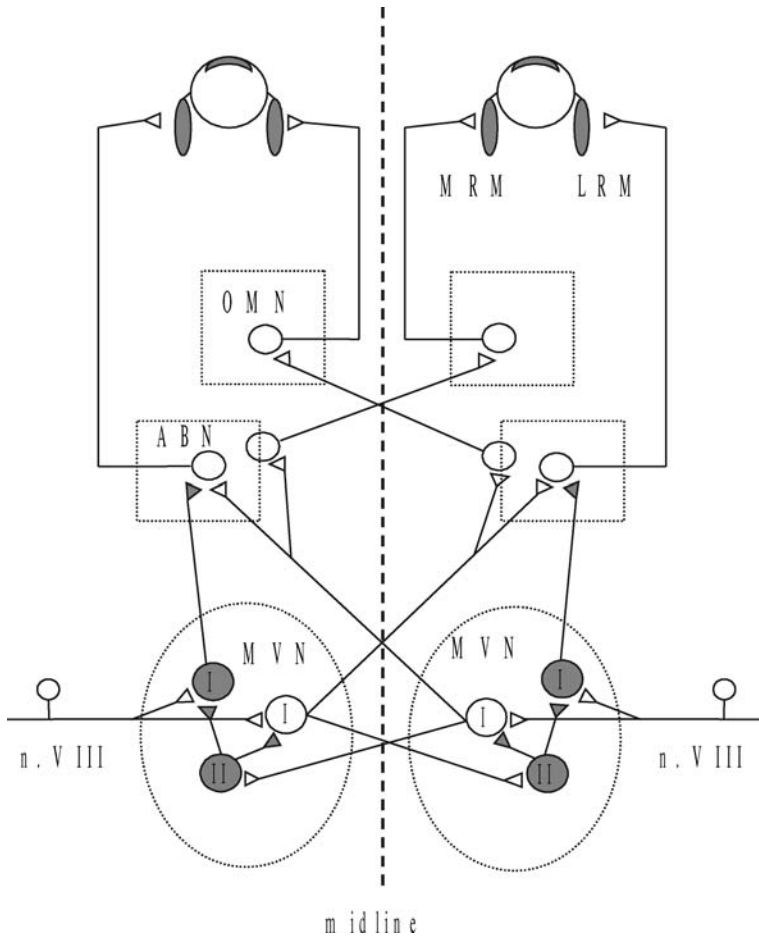
Figure 1: Basic hVOR network. Schematic diagram of the organization of the medial vestibular nucleus (MVN) projections involved in mediating the horizontal vestibulo-ocular reflex (hVOR). Primary vestibular afferents from the horizontal semicircular canals travel in the VIIIth cranial nerve (n.VIII) and synapse with second-order, type I MVN neurons in the brainstem. Type II MVN neurons are inhibitory interneurons, which receive excitation from the contralateral MVN. Connections between the MVN neurons of the left and right sides form a reciprocal, commissural inhibitory system. Projections of the type I MVN neurons to the abducens nucleus (ABN) and thence to the oculomotor nucleus (OMN) lead to the reflex activation of the medial and lateral rectus muscles (MRM and LRM, respectively). The neurons actually simulated are type I excitatory MVN neurons, which are the key middle neurons in the reflex arc. Shaded neurons and synapses are inhibitory.

pathway that mediates online feedforward eye movement responses to head rotation in the horizontal plane.

Experimental studies of MVN neurons in slices have shown that these neurons are intrinsically active, with pacemaker-like membrane conductances that generate a regular, spontaneous resting discharge in vitro (review, Straka, Vibert, Vidal, Moore, & Dutia, 2005). Comparison of the in vitro and in vivo activity of MVN neurons in rodents shows that the spontaneous firing of MVN cells in slices is about 50% of their firing rate in vivo (Ris & Godaux, 1998). It is now widely accepted that the in vivo spiking activity of MVN neurons is the result of the interaction between their basal spontaneous pacemaker-driven firing and the excitatory and inhibitory synaptic inputs they receive from various sources. Computational (Av-Ron & Vidal, 1999) and slice (du Lac & Lisberger, 1995; Ris et al., 2001) studies of single MVN neuron response in rodents have reported a limited range of frequencies and amplitudes of input for which single neuron response is linear and follows the input accurately.

In vivo experiments in the monkey show that the VOR is linear, has a very short latency, and is accurate up to 20 Hz (Huterer & Culleen, 2002) and beyond (Ramachandran & Lisberger, 2005). Assuming similar response properties for rodent and monkey neurons, single neuron responses can thus not account for the behavioral responses. Some recent studies have included realistic neurons in cellular network models (e.g., Cartwright et al., 1999, 2003). These models have not, however, included the intrinsic activity of MVN neurons and do not account for the full range of real-world VOR performance.

Because the pacemaker currents in each individual MVN neuron are independent, their mean rates are heterogeneous, and hence timing of spiking activity in the population of MVN neurons is likely to be largely asynchronous. Additional factors promoting asynchronous firing in MVN neurons include the independent timing of spiking activity in their main excitatory input from vestibular nerve afferents and in the inhibitory inputs they receive from interneurons in the vestibular commissural system (see Figure 1). Collectively the fluctuations from such independent synaptic inputs have been termed integration or diffusive noise (Gerstner, 2000). Here we investigate the hypothesis that diffusive noise and the intrinsic spontaneous activity of MVN hVOR neurons, by enhancing asynchrony in MVN population activity, enable the high-fidelity linear response of the hVOR.

## 2 Model

**2.1 Simulation Design.** We simulated a population of 500 integrate-and-fire neurons, representing type I MVN neurons receiving a common vestibular input (e.g., from horizontal semicircular canal afferents; Figure 1), and measured their population response and synchrony under various conditions. For the purpose of this study, we employed a generic population of homogeneous neurons with an input resistance $R_m = 100$ MΩ, a membrane

time constant $\tau_m = 20$ ms, a resting potential $E_{rp} = -60$ mV, firing threshold $V_{th} = -50$ mV, and 1 ms absolute refractory period. The membrane potential for neuron $i$, $V_i$, evolved according to

$$\tau_m \frac{dV_i(t)}{dt} = E_{rp} - V_i(t) + R_m (I(t) + P_i + \varepsilon_i(t)).$$

$$I(t) = I_0 + i(t) \quad P_i = N(\mu, \sigma_2) \quad \varepsilon_i(t) = N(0, \sigma_1).$$

To model potentially diverse spontaneous activity, a constant "pacemaker" current, $P_i$, for each neuron was chosen independently from a gaussian distribution, $N(\mu, \sigma_2)$. Diffusive noise was simulated by independently injecting each neuron with low-pass filtered gaussian noise, $\varepsilon_i(t)$, with a 2 ms time constant. The vestibular input signal $I(t)$ is directly injected to all neurons simultaneously. The resting input level $I_0$ simulated the steady input from vestibular afferents in the head-stationary condition, while dynamic input from head movement acts via $i(t)$. At initialization, the membrane potentials of the MVN neurons were assigned random values between $E_{rp}$ and $V_{th}$ from a weighted distribution calculated to give a stable spontaneous population activity over time as described in detail by van Rossum (2001). To further ensure the forgetting of initial conditions, in each simulation the population activity was allowed to settle for 2 seconds under constant resting input ($i(t) = 0$) before application of a dynamic input signal and recording of results. In simulations where diffusive noise $\varepsilon(t)$ was kept at zero, the noise standard deviation was annealed down from an initial value of $\sigma_1 = 5$ pA to zero during the first second after initialization.

**2.2 Analysis of the Population Response to Head Velocity Inputs.** The population response to input was obtained by binning the spikes of all the neurons in the population into 5 ms fixed width bins over the duration of the simulation (where 5 ms bin size is chosen to correspond to the typical postsynaptic integration time). The input current stimulus was also binned into corresponding 5 ms bins. To quantify the fidelity of signal transmission, the mean absolute difference between the input and output bins was calculated over the simulation period, after normalizing the input current and output spikes relative to their own variance. Fidelity of signal transmission was expressed as one minus the mean error over the simulation period, with the maximum value of 1 corresponding to a perfect match between input and output bins. The population response is an appropriate representation for the output of this pathway, as there are no further interneuron layers to decode any potential complex population code since MVN neurons converge directly on abducens motoneurons.

An alternative performance measure for sinusoidal signals consists of fitting sinusoids to both the input and output and evaluating their relative gain and phase difference (Ramachandran & Lisberger, 2006). However, our nonparametric fidelity measure is sufficient insofar as if either the gain or phase is distorted, fidelity will also be degraded. Moreover, it is particularly

appropriate here, as we will evaluate the performance under more natural noisy multifrequency input for which sinusoid fitting is inappropriate.

The degree of synchrony in the population of MVN neurons over the simulation period was quantified using a variant of the synchronization index of Burkitt and Clark (2001; Goldberg & Brown, 1969). Each of $N$ neurons defines a unit length vector of phase angle ($a_i$) determined by the position of its current membrane potential ($V_i$) in the range between resting potential and firing threshold:

$$a_i = \frac{2\pi V_i}{V_{th} - E_{rp}}$$

$$s = \sqrt{\left(\sum_i \cos(a_i)/N\right)^2 + \left(\sum_i \sin(a_i)/N\right)^2}.$$

The mean vector of the population distribution is calculated, the magnitude of which defines a synchronization index ($s$) between one and zero. If all the neurons have the same membrane potential and hence phase angles, their unit vectors align, and the magnitude of the population mean vector tends toward 1. Alternatively, if the neurons have a uniform distribution of membrane potentials, their unit vectors are uniformly distributed in phase, and the magnitude of the population mean vector therefore tends to 0. A synchronization index of 1 thus represents perfect synchronization of state, and an index of 0 represents uniform distribution of neural states and complete asynchrony. Population asynchrony is defined as 1 minus the synchronization index $s$. Given this instantaneous measure of synchrony, the synchrony for an entire simulation was simply defined as the mean of the index over all time steps. Alternate synchronization measures compute the phase alignment between spikes and a sinusoidal input (e.g., Ramachandran & Lisberger, 2006). In contrast, our measure essentially evaluates the probability distribution over membrane potentials in the population, with a uniform distribution corresponding to perfect asynchrony and a delta function distribution corresponding to perfect synchrony. This is motivated by the finding that fast, efficient population rate code transmission occurs in the domain when the distribution over membrane potentials is more uniform than peaked (van Rossum et al., 2002). Our procedure generalizes spike-based measures, since correlated spikes occur as the immediate result of correlated membrane potentials. The benefits of this measure are that synchrony can be quantified in response to nonperiodic input as well as under conditions of few or no spikes where, for example, the entire population may be silent or refractory.

## 3 The Independent Effects of Diffusive Noise and Pacemaker Activity on the Population Response

**3.1 Population Response Rate Coding.** To parameterize our model, we use data from the alert monkey (Chen-Huang, McCrea, & Goldberg,
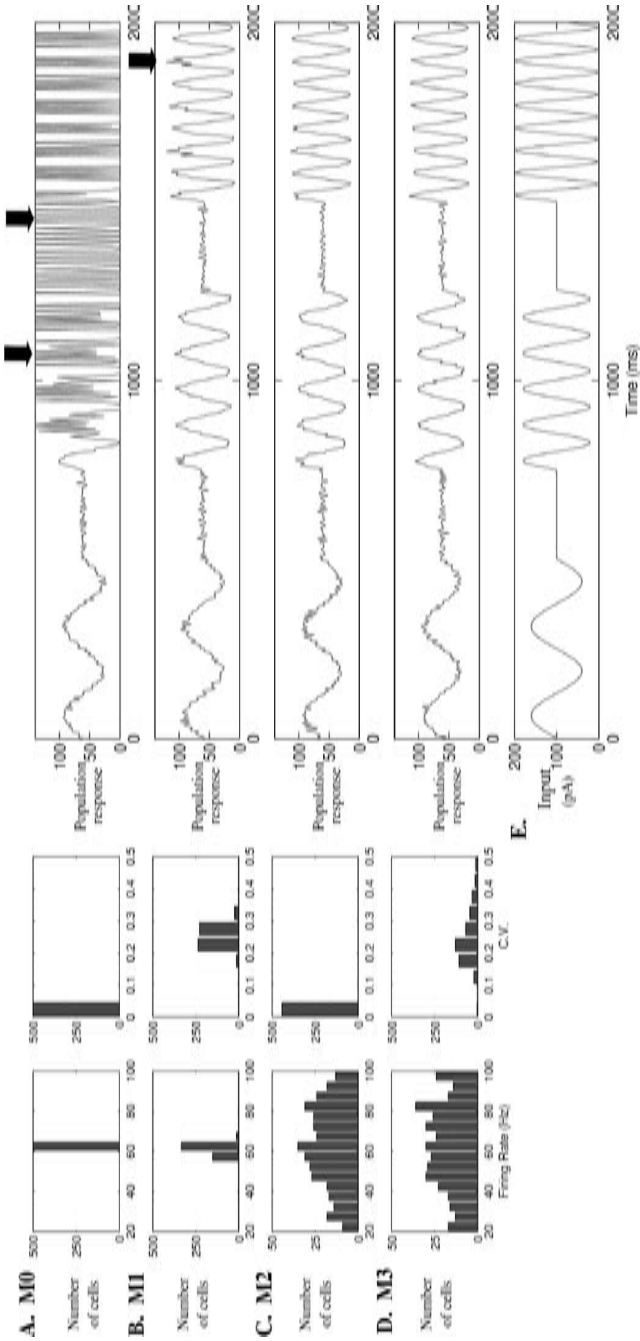
1997) in which a population of vestibular type I cells was observed to fire with rate $(62 \pm 33)$ Hz and with mean interspike interval coefficient of variation (CV) of 0.29. We assume the variability in the mean rate to be due to heterogeneous innervation and pacemaker conductance strength. (However, the source of the heterogeneity does not matter for our purposes, and we model these effects together). The firing irregularity is assumed to be due to diffusive noise effects.

To separate the effects of diffusive noise and pacemaker activity on population response, we created four model variants. The most realistic model variant (model 3) included both diffusive noise and heterogeneous pacemaker activity. The parameters ($I_0 = 115$ pA, $\mu = 100$ pA, $\sigma_1 = 60$ pA, $\sigma_2 = 67$ pA) were chosen such that the population had resting firing statistics matching those observed in vivo as described above. The next model variant (model 2) included heterogeneous pacemaker activity but not diffusive noise by setting $\sigma_1 = 0$ pA, which eliminated irregularity in individual neurons firing rate. Model 1 included the effects of the diffusive noise input, but in a homogeneous population, by setting $\sigma_2 = 0$ pA. Finally, model 0 was a population of homogeneous noiseless neurons with ($I_0 = 115$ pA, $\mu = 100$ pA, $\sigma_1 = 0$ pA, $\sigma_2 = 0$ pA).

The resting statistics before driven input are shown in Figure 2 (left) and population activity in response to a sample input in Figure 2 (right). In

---

Figure 2: Comparison of mean spike firing rate (left) and coefficient of variation of interspike intervals, CV (middle) of the population of simulated MVN neurons in each model variant, for the head-stationary resting input condition, $i(t) = 0$. Population response to subsequent driven sinusoidal input at increasing frequencies and amplitudes (60 pA, 4 Hz; 80 pA, 10 Hz; 100 pA, 16 Hz)(right). The common input signal to all models $I(t)$ is shown in $E$. (A) In model 0, where the MVN neurons received no diffusive noise input and had identical pacemaker currents, the neurons initially all fire regularly and at the same average rate. For moderate inputs, the population activity in model 0 begins to synchronize, and the synchronous activity continues after the sinusoidal input has ended (arrows). (B) In model 1, the addition of diffusive noise causes neurons to fire irregularly, but with similar average firing rates. It initially fires asynchronously and reflects the input well throughout the period in which model 0 becomes synchronized. For the highest amplitude and frequency, there is still a slight tendency, to synchronize (arrow). (C) In model 2, where the MVN neurons received no diffusive noise inputs but had heterogeneous pacemaker current amplitudes, the neurons exhibit a wide spread of mean rates across the population but fire regularly. Good response is maintained throughout driven input. (D) In model 3, where the MVN neurons received diffusive noise inputs and had heterogeneous amplitudes of pacemaker currents, there is both a spread in mean rate and irregularity in firing. Good response is maintained throughout driven input.

all four models the neurons initially fired asynchronously, with population synchrony $s < 0.25$, because of their random initialization. The neurons in model 0 (see Figure 2A) initially fired regularly and at the same mean discharge rate, reflecting their identical pacemaker current inputs and lack of diffusive noise. In model 1, the neurons initially fired less regularly due to the effects of the diffusive noise input $\varepsilon_i(t)$, but had similar average firing rates since they received the same pacemaker current injection $P_i$ (see Figure 2B). By contrast, the neurons in model 2 initially discharged regularly because of the lack of diffusive noise, but at different average rates because each neuron received an independently selected amplitude of pacemaker current. The neurons in model 3 fired irregularly and at different average rates because they received both diffusive noise and heterogeneous pacemaker currents (see Figure 2D).

A driving input containing sinusoids of increasing amplitude and frequency was next applied (see Figure 2E). In response to the smallest input sinusoid (60 pA, 4 Hz), all four models generated a population response that represented the input fairly well. However, in response to the next input sinusoid (80 pA, 10 Hz), the neurons in model 0 rapidly synchronized, and the population response no longer represented the input signal. The synchronous firing continued even after the end of the sinusoidal input (see Figure 2A, arrows). By contrast, the neurons in models 1 and 2 showed much greater resistance to synchronization, and the population response showed a good sinusoidal modulation over amplitudes and frequencies of input. In response to the the final input sinusoid (100 pA, 16 Hz), however, model 1 again showed a small tendency to synchronize (see Figure 2B, arrow), suggesting that, for stronger driving inputs, the diffusive noise alone is less effective in resisting aliasing compared to the intrinsic pacemaker current inputs in model 2. In model 3, where the neurons received both diffusive noise and heterogeneous pacemaker current amplitudes, the population response best followed the input signal over the sample amplitudes and frequencies.

To understand more clearly how the population rate code works, consider Figure 3 which shows a more detailed segment of activity from the 500 cells in model 0 and model 3 configurations responding to the 16 Hz frequency, 100 pA amplitude input. Normalized instantaneous frequency (defined as $1/(t_2 - t_1)$, given spikes at times $t_1$ and $t_2$) is plotted against spike time along with the input in Figure 3 (top). In Figure 3A, spikes from model 0 (synchronization index, $s = 0.6$) tend to occur synchronously with each other and at points phase-locked with the input. (There are 150 overlapping spikes at only 25 unique times in this plot.) There are extensive periods of input with no spikes at all, during which downstream neurons have no information about the activity of the input. In model 3 (see Figure 3B, $s = 0.14$), the population's spike frequencies as a whole are modulated by the input much more smoothly in time and frequency. We also plot the population response based on 10 randomly selected cells (broken line)
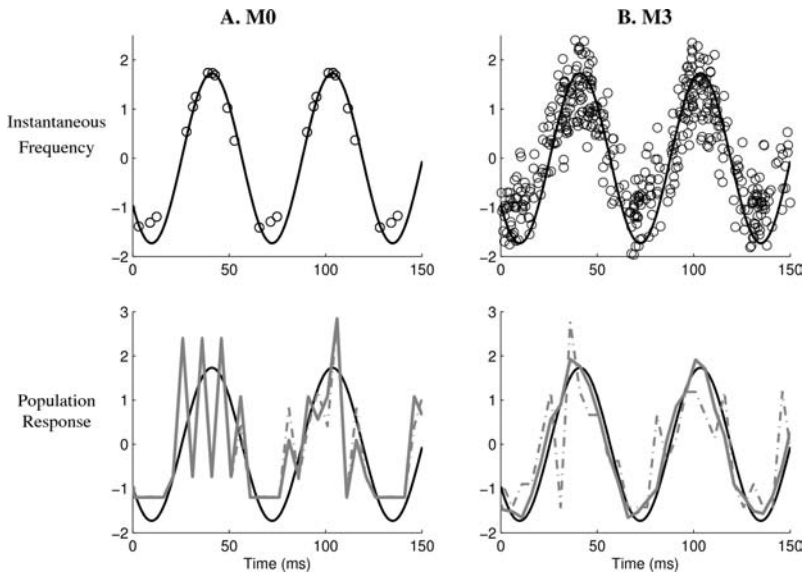
Figure 3: Detailed activity sample of cells in response to sinusoidal input and the resulting population response rate code. (A) Top: The synchrony ($s = 0.6$) in spiking activity in model 0 is clear with the overlapping, phase-locked spike times (circles). As a result, the input (thin line) is therefore poorly represented by the instantaneous spike times. Similarly, the population response does not track the signal well (bottom). Furthermore, the population response does not improve when the number of cells is increased from 10 (broken line) to 500 (thick line). (B) The asynchrony ($s = 0.14$) and noise in spiking activity in model 3 spread the spikes in time and around the input amplitude. The population response of 10 cells provides a coarse representation of the input, but the response of 500 cells is a good representation of the input. In the upper spike plots, only spikes from a random 50 cells are plotted to keep the model 3 figure clear; however, considering all 500 cells' spikes for model 0 does not reveal any new, unique spike times. Input is 16 Hz frequency, 100 pA amplitude.

and of all 500 cells (unbroken line) for each model along with the input. In model 0, the population response does not reflect the input well, and this does not change significantly when considering 10 or 500 cells. This is because the synchronously firing cells are all firing at similar times, so adding further cells doing exactly the same thing carries no further information. In model 3, because of the cells' asynchronous firing times, the full 500-cell response reflects the input much more clearly than either the population response of a random 10-cell subset or an individual cell's instantaneous frequency. The signal is therefore carried not by the activity of any single cell but by the mean rate of the whole asynchronous population,

which allows transmission fidelity to increase with the number of cells.

**3.2 Effects of Input Amplitude and Frequency.** Next we quantified the performance of each model as a function of both input amplitude and frequency. Each model was simulated for 6 s of driven sinusoidal input of fixed amplitude and frequency. The input frequencies were varied logarithmically between 0.5 and 20 Hz to emulate the physiological operating range of the mammalian (monkey) VOR (Huterer & Cullen, 2002). The amplitude $|i(t)|$ of the sinusoidal input was varied in 10 pA steps between 10 pA and 100 pA. This caused modulations in firing frequency of the neurons from the barely significant at 10 pA to modulations of $\pm 50$ Hz at 100 pA, which was just small enough to avoid inhibitory cut-off and silencing of the 62 Hz resting rate during the contraversive half-cycle of head rotation. For each model variant, the mean fidelity and synchrony over the course of each simulation are illustrated in Figure 4. In model 0 (see Figure 4A), although the population is initialized randomly and asynchronously, it rapidly synchronizes in response to the input, particularly at the highest input frequencies and amplitudes. As a result, transmission fidelity for these inputs is poor. By contrast, in models 1 and 2, the diffusive noise input and pacemaker-current injection, respectively, are more effective in maintaining population asynchrony over the whole input range (see Figures 4B and 4C). However, in model 1, signal transmission fidelity falls off slightly at the highest amplitudes and frequencies (see Figure 4B, arrow). In model 3, where the neurons receive both diffusive noise and pacemaker-current injection, synchrony is the lowest and signal transmission fidelity most robust throughout the input parameter space, including the highest and lowest amplitudes and highest frequencies (see Figure 4D). In all cases, there is a reduced fidelity at the lowest amplitudes because the input-related response component becomes smaller with respect to stochastic fluctuations in the output, and hence the baseline error is increased compared to the higher amplitudes. The differences in performance between model 0 and models 1 to 3 illustrate the importance of asynchronous neuronal activity in maintaining population response fidelity over a wide range of input frequencies and amplitudes.

## 4 Continuous Dependence of Population Response on the Effects of Diffusive Noise and Pacemaker Activity

**4.1 Sinusoidal Input.** We wondered how the signal fidelity and population asynchrony depended on the exact amount of diffusive noise and the range of pacemaker currents. We measured the population response behavior for three frequencies of vestibular input (see Figure 5). Three input signal frequencies were tested from the low, middle, and high regions
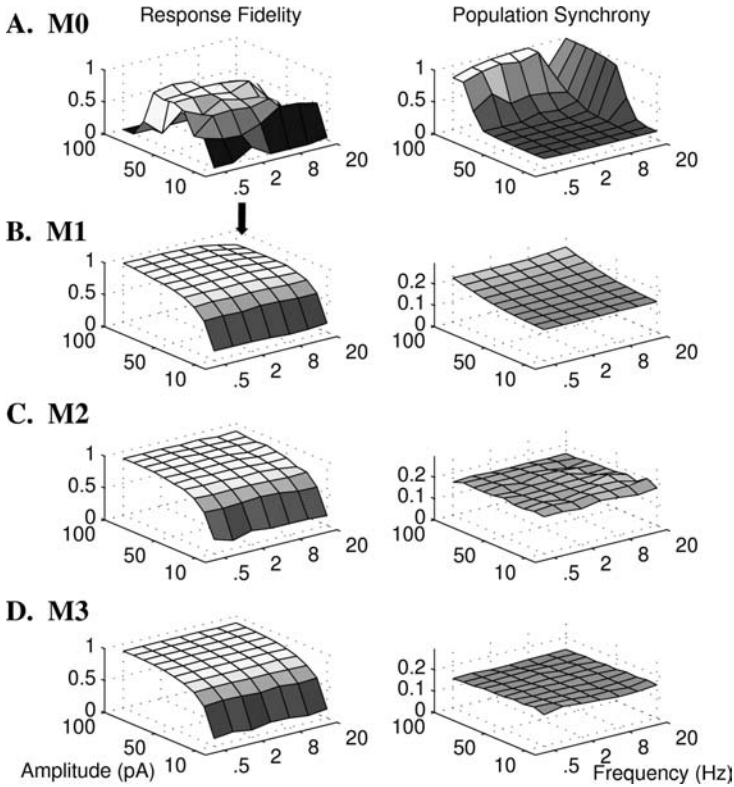
Figure 4: Dependence of response fidelity and population asynchrony on amplitude and frequency of signal input. Transmission fidelity (left) and population asynchrony (right) for model variants in response to a sinusoidal vestibular input $i(t)$ of varying amplitude and frequency; $y$-axes: amplitude of periodic input $i(t)$; $x$-axes: frequency of periodic input. (A) For model 0 (homogeneous, noiseless neurons), the synchrony is high and the population response fidelity poor, particularly at the highest amplitudes and frequencies. (B) Model 1 (homogeneous neurons with diffusive noise) fidelity falls off at higher frequencies and amplitudes (arrow). In (C) model 2 (heterogeneous neurons with no diffusive noise input) and (D) model 3 (heterogeneous neurons with diffusive noise input), high fidelity and asynchrony are maintained across the parameter space. The data shown are averages for each simulation over 6 s of sinusoidal-driven input after settling.

of the physiological range (0.5, 8, 20 Hz), while the amplitude of the input signal was fixed at 100 pA (±50 Hz firing rate modulation). The standard deviation of the diffusive noise input ($\sigma_1$) and pacemaker current heterogeneity ($\sigma_2$) were increased in 10 pA steps from 0 to 110 pA. This produced a range of simulations with resting statistics from 0 CV and rate
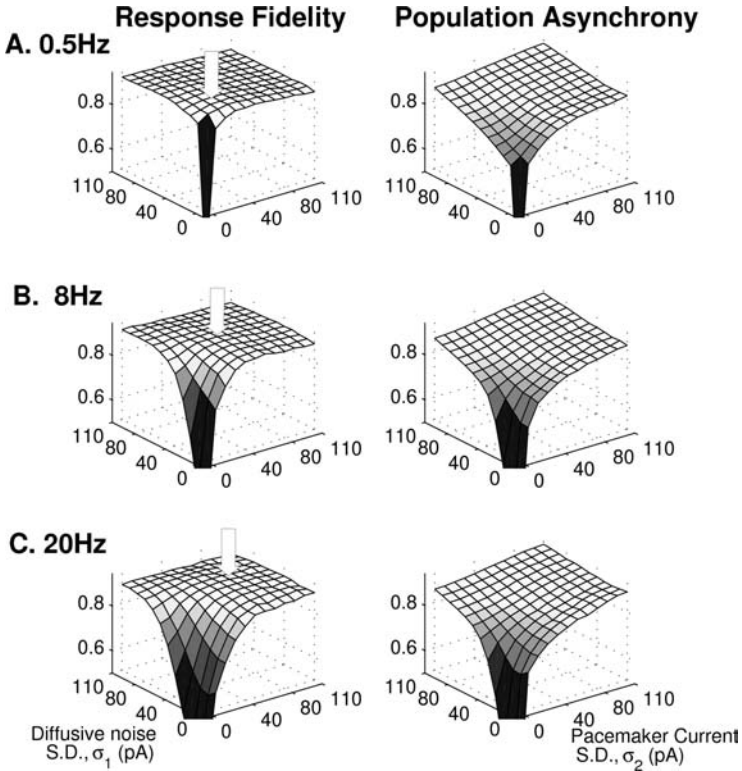
Figure 5: Dependence of response fidelity and population asynchrony on diffusive noise inputs and pacemaker currents; $x$-axes: diffusive noise standard deviation, $\sigma_1$. $y$-axes: pacemaker current amplitude standard deviation, $\sigma_2$. (A–C) Fidelity and asynchrony for signal input frequencies of 0.5, 8.0, and 20.0 Hz, respectively. Asynchrony and fidelity increase rapidly from the origin with small additions of diffusive noise or pacemaker currents in all three cases. In each case, moderate levels of diffusive noise and pacemaker current heterogeneity yield optimal response fidelity; increases in either parameter beyond these values lead to an increase in asynchrony and a decline in fidelity. For higher-input frequencies, peak response fidelity is achieved at higher values of diffusive noise and pacemaker current heterogeneity (arrows, left column). Each point shown is the result averaged over five independent simulations, each of 2 s length with the corresponding parameters $\sigma_1$, $\sigma_2$ and driven sinusoidal input of 100 pA amplitude.

standard deviation to 0.46 CV and 51 Hz rate standard deviation. Within this spectrum of parameters, the simulation equivalent to model 0 lies at the origin of the plots. Models 1 and 2 lie along the $y$- and $x$-axes, respectively. An interior point corresponds to the model 3 configuration.

As expected, at low values of either diffusive noise or pacemaker current heterogeneity, the simulated neurons were prone to synchronization, and signal transmission fidelity was poor. Particularly for the low-input signal frequency of 0.5 Hz (see Figure 5A), even small additions of diffusive noise or pacemaker current heterogeneity resulted in a significant increase in the population asynchrony maintained and a corresponding large increase in fidelity. In the midfrequency range (8 Hz; see Figure 5B) and the high-frequency range (20 Hz; see Figure 5C), fidelity again showed a rapid improvement with the addition of small to moderate levels of diffusive noise or pacemaker current heterogeneity. In both cases, increasing pacemaker current heterogeneity was more effective and led to a steeper increase in fidelity than the addition of diffusive noise. For each input frequency tested, there was a shallow peak of optimum transmission fidelity associated with a plateau in asynchrony in the midrange values of diffusive noise and pacemaker current amplitudes (see Figure 5, arrows). Beyond the optimum area of fidelity, the benefits of further increase in asynchrony were outweighed by progressively more noise-driven, noninput-related spiking. The distance from the origin of the peak region of transmission fidelity increased with input signal frequency (see Figure 5, arrows). Since the neural populations were more prone to synchronization in response to higher-frequency inputs, higher values of diffusive noise and pacemaker current heterogeneity were required to obtain peak asynchrony and fidelity at high-input signal frequencies (e.g., Figure 5C versus 5A).

**4.2 Diffusive Noise and Pacemaker Current Levels Yielding Optimum Population Response to Multiple-Frequency Input Signals.** Given the strong dependence of optimum tuning on input frequency, we investigated the levels of diffusive noise and pacemaker heterogeneity required for optimum response of the simulated MVN neurons to input of more biologically relevant statistics than pure sinusoids. To do this, we constructed a random input signal with exponentially decaying (10 ms time constant) power spectrum, similar to that observed for voluntary motion in monkeys (Huterer & Cullen, 2002). Figure 6A illustrates the resulting fidelity surface for the the population. The best-performing simulation—with best match between input and output population response—is at $\sigma_1 = 50$ pA, $\sigma_2 = 50$ pA (see Figure 6A, black arrow). The simulation with the most biologically realistic statistics (i.e., nearest to model 3) is at $\sigma_1 = 70$ pA, $\sigma_2 = 60$ pA (see Figure 6A, white arrow).

As this is our analysis of main quantitative interest, we also increase the biological realism of the neurons incrementally. The adaptive properties of MVN neurons have been extensively studied in the literature. In particular, they are known to exhibit postinhibitory rebound firing (PRF) and firing rate adaptation (FRA) (Straka et al., 2005). We did not expect a strong quantitative effect as the time constant of adaptation is on the order of 1 second, which is much longer than the time constant of the input signal. For
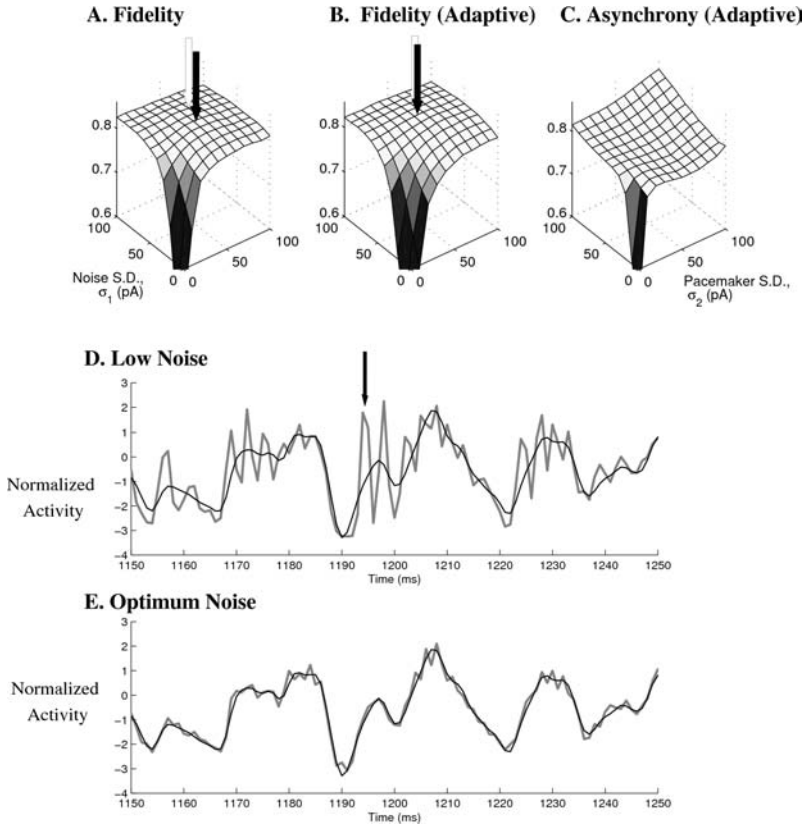
Figure 6: Response to multiple-frequency biologically relevant inputs suggests the diffusive noise and pacemaker parameters are tuned for optimal performance in vivo. Simple integrate-and-fire neurons (A); neurons with postinhibitory rebound firing and firing rate adaptation (B–E). Dependence of fidelity (A, B) and asynchrony (C) on diffusive noise and pacemaker currents using multiple frequency input signals. Peak fidelity (black arrows) is obtained using parameters (A, $\sigma_1 = 50$ pA, $\sigma_2 = 50$ pA; B, $\sigma_1 = 60$ pA, $\sigma_2 = 50$ pA) that are very close to those that produce best fit to firing rate standard deviation and interspike interval coefficient of variation of MVN neurons in vivo (A, B; white arrows, $\sigma_1 = 70$ pA, $\sigma_2 = 60$ pA). (D) Sample of normalized population firing activity (thick line) in response to multiple frequency vestibular input $i(t)$ (thin line), for a model MVN using low values for diffusive noise variance and pacemaker current heterogeneity ($\sigma_1 = 10$ pA, $\sigma_2 = 10$ pA). Arrows indicate bursts of synchronous firing followed by refractory effects that markedly impair the fidelity with which the population activity follows the input signal. (E) The optimal values found for diffusive noise variance and pacemaker current heterogeneity yield a population response that follows the input signal with highest fidelity.

completeness, we nevertheless implemented these as described in detail by Sekirnjak and du Lac (2002). Figures 6B and 6C illustrate the fidelity and asynchrony surfaces for the adaptive population. In this case, the highest-fidelity simulation was at $\sigma_1 = 60$ pA, $\sigma_2 = 50$ pA (see Figure 6B, black arrow).

In both cases, the close match between the best-performing simulation and the simulation best matching the biological statistics suggests that the in vivo system is broadly tuned to optimize transmission fidelity. As expected, the difference between the locations of the optimal adaptive (see Figure 6B) and nonadaptive (see Figure 6A) simulations was not large. The optimal adaptive simulation was slightly closer to the most realistic simulation. Every point on surfaces in Figures 6A to 6C is an average over six independent simulations of 6 s length after 2 s of settling.

Sections of activity for the simulated adaptive neurons with low levels of diffusive noise and pacemaker current heterogeneity (see Figure 6B, first internal square; $\sigma_1 = 10$ pA, $\sigma_2 = 10$ pA) and for neurons in the optimal configuration are illustrated in Figures 6D and 6E. In the low-noise case, the population response broadly followed the input signal but was markedly distorted by a tendency to synchronous bursting activity (see the arrow, Figure 6D). By contrast, with moderate levels of diffusive noise and pacemaker current heterogeneity ($\sigma_1 = 60$ pA, $\sigma_2 = 50$ pA), the population response provided a much more faithful representation of the input signal (see Figure 6E).

## 5 The Commissural Inhibitory System and Population Asynchrony in MVN Neurons

To investigate the contribution of the reciprocal commissural inhibitory connections between the bilateral MVNs (see Figure 1) on signal transmission, the simulations were repeated using two interconnected nuclei. The second nucleus was stimulated with the same mean input signal $I_0$ as the first, but with the dynamic component $i(t)$ inverted. The nuclei are connected via type II interneurons (see Figure 1), but we abstract their contribution by directly connecting the nuclei in an all-to-all manner and delaying spikes with the biologically observed 3 ms latency delay. Synapses are modeled single exponential decay with 5 ms time constant, approximating the time constant in vivo. The resting $I_0$ input and synaptic strengths were scaled such that the firing rate of 62 Hz with commissural inhibitory input was a 22% reduction of the spike rate that would otherwise be observed without the commissural connections (Ris & Godaux, 1998).

We compared the population responses of one MVN to sinusoidal head velocity inputs with and without commissural inhibitory inhibition, using either a pair of MVNs with minimal diffusive noise ($\sigma_1 = 5$ pA) or a pair of MVNs in the most biologically realistic model 3 configuration. Using a single input frequency of 2 Hz for clarity, Figure 7 illustrates that the linking
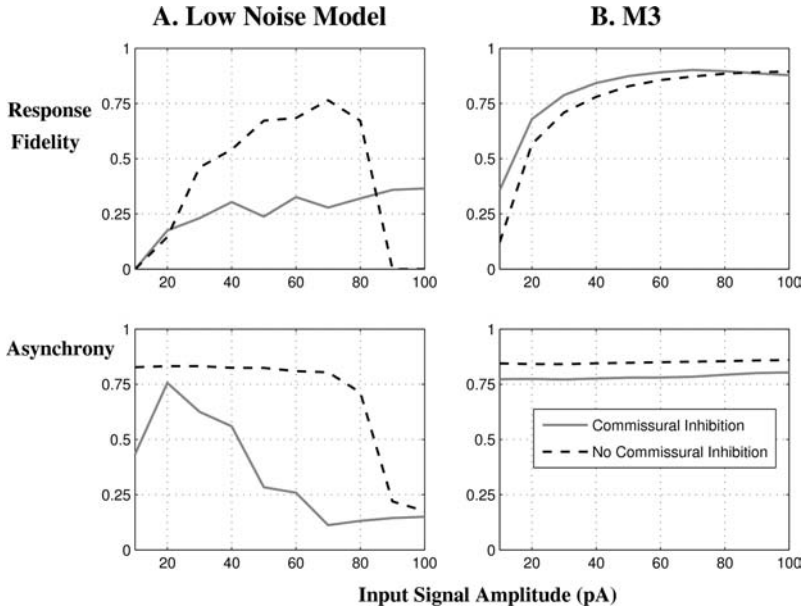
Figure 7: Effects of commissural inhibition on population asynchrony and response fidelity in a bilateral, reciprocally connected model containing two MVNs. (A) Low-noise model with $\sigma_1 = 5$ pA shows a loss of fidelity and asynchrony with input amplitudes larger than about 80 pA (dashed lines). When two model 0 configuration MVNs are connected by a reciprocal commissural inhibitory system,there is a marked deterioration of fidelity and asynchrony (solid line). (B) Model 3,with heterogeneous neurons and diffusive noise, maintains high fidelity and asynchrony for all input amplitudes in both the isolated and commissurally connected simulations. In the presence of commissural inhibition, asynchrony is maintained, and differential amplification provided by the commissural system yields a higher fidelity than in the isolated model 3 MVN.

of two MVNs via a commissural inhibitory connection had a markedly deleterious effect on the response characteristics of low-noise MVNs but a beneficial effect on the response characteristics of the biologically realistic MVNs.

In the absence of the inhibitory commissural connection (see Figure 7A, dashed lines), the population response showed asynchrony and fair fidelity over a relatively restricted range of input signal amplitude, with a loss of asynchrony and drop in fidelity at input amplitudes greater than 80 pA. However, in the presence of the inhibitory commissural connection (see Figure 7A, continuous lines), there is a much more precipitous loss of asynchrony and generally poorer population response fidelity, because the

closed-loop inhibitory system tends to promote the synchronization of neuron firing through the timing of its inhibitory inputs to the MVN neurons. By contrast, in the model 3 configuration, where asynchrony and response fidelity in the isolated MVNs are more robust over the entire amplitude range (see Figure 7B, dashed lines), the addition of a commissural inhibitory connection results in only a small reduction in asynchrony (see Figure 7B) as the synchronizing tendency is counteracted by the diffusive noise and pacemaker currents. As they are able to resist dramatic synchronization, the model 3 neurons are able to exploit the differential amplification offered by the commissural inhibitory connection. This increases in fidelity at all amplitudes, particularly at small input amplitudes where signal-to-noise ratio is lowest and the amplification is most beneficial. A similar improvement of population response fidelity is seen for all frequencies (0.5–20 Hz) tested in model 3 neurons connected by an inhibitory commissural connection.

## 6 Discussion

**6.1 Population Asynchrony and Signal Transmission Fidelity.** In this study we have investigated the importance of asynchronous firing in a population of simulated neurons for the fidelity of signal transmission over a range of input amplitudes and frequencies, using the mammalian VOR pathway as an exemplar model system in which fidelity of brainstem MVN neurons is critical for accurate gaze stabilization. Our findings show that asynchrony in population activity, due to either diffusive noise inputs or the intrinsic, spontaneous activity of MVN neurons, is effective in maintaining a high-fidelity population response over a wide operating range. In particular, in the absence of both diffusive noise and pacemaker activity, the simulated MVN neurons show a strong tendency to synchronize in response to common input signals of moderate frequencies and amplitudes so that their signal transmission capacity is limited to a small range of low-frequency, medium-amplitude inputs. The presence of either diffusive noise or independent pacemaker currents in the individual MVN neurons results in a marked improvement in the operating range over which the population response is modulated with high fidelity, as they counter the MVN neurons' tendency to synchronize with each other and phase lock with the input signal. While the addition of either diffusive noise or pacemaker activity improves signal transmission fidelity, optimal performance extending to higher-input amplitudes and frequencies is obtained in a model where moderate levels of both diffusive noise and pacemaker currents are present (see Figure 5). Further increases in either the diffusive noise or the strength of pacemaker currents beyond optimal levels results in a deterioration of population response fidelity because this increases stochastic, non-input-related spiking in the MVN neurons (see Figure 5). Moderate levels of both diffusive noise and pacemaker currents appear to

act synergistically to generate population asynchrony and optimal response fidelity, without either one being large enough to add excessive stochastic firing.

Interestingly the values of diffusive noise and pacemaker activity that yield optimal fidelity of biologically relevant signal transmission in the simulated MVN neurons are similar to those that give a good approximation of the mean firing rate and CV of MVN neurons in vivo (see Figure 6). This correspondence, despite the approximations and assumptions in our models, suggests that both diffusive noise and pacemaker-current heterogeneity are likely to be functionally important in maintaining the asynchrony and population response behavior of MVN neurons in vivo and that these are broadly tuned to yield optimal fidelity.

These findings are in line with previous theoretical work in which diffusive noise was used to maintenance of asynchrony among spiking neurons (Knight, 1972; Gerstner, 2000; van Rossum et al., 2002). Heterogeneity among neurons was shown to have a similar effect on synchrony (Masuda & Aihara, 2003; Masuda et al., 2005). Here we find that combining both is optimal to achieve a short-latency, high-fidelity encoding of a common input signal in a population rate code. Such signal transmission characteristics are highly appropriate for the mammalian VOR, which is characterised by high-fidelity, phase-aligned eye movement response with near unity gain at up to 20 Hz for voluntary and externally applied head-on body rotations (Huterer & Cullen, 2002) and beyond 20 Hz for externally applied whole body rotations (Ramachandran & Lisberger, 2005). This performance is in marked contrast, however, with electrophysiological properties of single MVN neurons. The frequency range over which individual MVN cells are able to respond to sinusoidal current injection without phase locking is limited to about 10 to 12 Hz, and at the higher frequencies only for very small input current amplitudes (du Lac & Lisberger, 1995; Av-Ron & Vidal, 1999; Ris et al., 2001). Although these studies are based on avian and rodent cell types, our own simulations indicate that in the absence of noise, primate neurons are also vulnerable to phase locking and synchronization at higher frequencies and amplitudes (see Figure 3A).

In this work, we have approximated the input as a continuous quantity directly proportional to head velocity, which is an obvious simplification. In particular, it has been shown that some individual vestibular afferent neurons phase-lock to the stimulus at higher frequencies, although they do not particularly synchronize with each other (Ramachandran & Lisberger, 2006). This does not change the argument presented here. However, depending on the pattern of innervation, more heterogeneity and diffusive noise may be required to resist synchronization by the phase-locked input. Interestingly, consistent with our model, the abducens neurons do not show phase locking (Ramachandran & Lisberger, 2006).

On the basis of our analysis, we suggest that the necessary wide frequency response of the hVOR system is therefore not achieved by firing rate

encoding of head velocity at the single-neuron level but by the population rate response of the asynchronously firing MVN neurons. This is consistent with a convergent innervation of abducens motoneurons by hVOR MVN neurons, so that each abducens motoneuron receives inputs from many MVN neurons. Abducens neurons are therefore well positioned to derive the integrated population response of the MVN cells.

**6.2 Intrinsic Excitability of MVN Neurons.** Our results suggest a novel biologically plausible role for the intrinsic, pacemaker-driven spontaneous activity of these neurons that has been extensively characterized in slice preparations of the MVN in vitro (see Straka et al., 2005, for a review). This interpretation predicts that multicellular recordings of MVN cells in vivo should observe asynchronous activity and that pharmacological blockade of pacemaker activity should dramatically degrade VOR performance. It is notable that other neuron types also concerned with vestibular-related signals, including prepositus hypoglossi neurons (Serafin, Vibert, de Waele, Vidal, & Muhlethaler, 1996) and nucleus gigantocellularis neurons (Serafin, Vidal, & Muhlethaler, 1996), have intrinsic membrane excitability and an in vitro spontaneous discharge analogous to that of MVN neurons (Straka et al., 2005). Thus, the ability to generate spontaneous intrinsic spiking activity, through the expression of pacemaker membrane conductances in individual neurons, may be a useful functional adaptation that promotes population asynchrony and a high-fidelity population response beyond that achieved by means of diffusive noise alone, appropriate for VOR dynamics over a wide operating range.

**6.3 Potential Functional Role of Subtypes of MVN Neurons.** In this study, we modeled a population of generic neurons rather than attempt to model more accurately the different ionic conductances of type A and type B MVN neurons (Serafin, de Waele, Khateb, Vidal, & Muhlethaler, 1991; Johnston, MacLeod, & Dutia, 1994; Cartwright et al., 1999, 2003). It has been proposed that differences in the active membrane conductances of type A and type B neurons may underlie frequency-specific tuning or resonance in the responsiveness of each of these subtypes (Ris et al., 2001; Straka et al., 2005). This proposition is compatible with our analysis. Since both type A and type B cells are spontaneously active and discharge at broadly similar firing rates in slice preparations in vitro, the above findings on population response behavior are likely to apply to both cell types. Indeed, it is an implicit corollary of the frequency-selective tuning of subtypes of MVN neurons (Straka et al., 2005) that the vestibular signal be encoded as a population response rather than in the firing rate of individual neurons in order to generate the required VOR performance over a wide frequency range.

Except for the comissural inhibitory connection, our study used only a single simple pathway. Other studies have tried to explain the detailed

behavioral idiosyncrasies of the mammalian VOR in terms of parallel pathways. For example, it has been suggested that the VOR is implemented by two parallel pathways. Ramachandran and Lisberger (2005, 2006) propose one fixed path and one plastic path, which can adapt to deal with changes in the lens or eye plant. Minor et al. (1999) propose one linear path and one nonlinear path. Such parallel path proposals are also compatible with our framework as either or both pathways could be instantiated by a population rate code such as we describe.

**6.4 MVN Population Asynchrony and the Vestibular Commissural Inhibitory System.** A prominent feature of the architecture of the VOR network in mammals is the reciprocal inhibitory commissure that links the MVN of the two sides (see Figure 1). We investigated the effects of linking two populations of simulated MVN neurons with a reciprocal inhibitory commissure and investigated the role of neuronal firing asynchrony in shaping the population response of the linked MVNs. In the absence of diffusive noise and pacemaker current heterogeneity in the MVN neurons, the effects of reciprocal commissural inhibition were to drastically reduce the already limited fidelity of the individual MVNs (model 0, Figure 7A). This presumably reflects the amplification by the closed-loop commissural system of the differential head velocity input signal applied to the bilateral MVN, which, in the absence of the randomizing effects of diffusive noise and pacemaker currents, also potentiates the tendency of the two populations of MVN neurons to rapidly synchronize so that signal transmission fidelity collapses. Remarkably, however, the addition of diffusive noise and pacemaker current heterogeneity to the MVN neurons leads to stable signal transmission and an improvement of population response fidelity (model 3, Figure 7B). Thus, diffusive noise and pacemaker heterogeneity in MVN neurons, by counteracting neuronal synchronization, enable the hVOR system to exploit differential amplification of the vestibular input signal by the commissural inhibitory system while maintaining population response fidelity over the required wide operating range. This further supports our proposed account of the high performance of the hVOR in vivo and of the role of intrinsic pacemaker-driven spontaneous activity of MVN neurons.

**References**

Arnold, D. B., & Robinson, D. A. (1997). The oculomotor integrator: Testing of a neural network model. *Exp. Brain. Res., 113*, 57–74.

Av-Ron, E., & Vidal, P. P. (1999). Intrinsic membrane properties and dynamics of medial vestibular neurons: A simulation. *Biol. Cybern.*, *80*, 383–392.

Burkitt, A. N., & Clark, G. M. (2001). Synchronization of the neural response to noisy periodic synaptic input. *Neural Computation*, *13*, 2639–2672.

Cartwright, A. D., & Curthoys, I. S. (1996). A neural network simulation of the vestibular system: Implications on the role of intervestibular nuclear coupling during vestibular compensation. *Biol. Cybern.*, *75*, 485–493.

Cartwright, A. D., Curthoys, I. S., & Gilchrist, D. P. (1999). Testable predictions from realistic neural network simulations of vestibular compensation: Integrating the behavioural and physiological data. *Biol. Cybern.*, *81*, 73–87.

Cartwright, A. D., Gilchrist, D. P., Burgess, A. M., & Curthoys, I. S. (2003). A realistic neural-network simulation of both slow and quick phase components of the guinea pig VOR. *Exp. Brain Res., 149*, 299–311.

Chen-Huang, C., McCrea, R. A., & Goldberg, J. M. (1997). Contributions of regularly and irregularly discharging vestibular-nerve inputs to the discharge of central vestibular neurons in the alert squirrel monkey. *Exp. Brain Res., 114*, 405–422.

Diesmann, M., Gewaltig, M. O., & Aertsen, A. (1999). Stable propagation of synchronous spiking in cortical neural networks. *Nature*, *402*, 529–533.

du Lac, S., & Lisberger, S. G. (1995). Cellular processing of temporal information in medial vestibular nucleus neurons. *J. Neurosci. 15*, 8000–8010.

Gerstner, W. (2000). Population dynamics of spiking neurons: Fast transients, asynchronous state, and locking. *Neural Computation*, *12*, 43–89.

Goldberg, J. M., & Brown, P. B. (1969). Response of binaural neurons of dog superior olivary complex to dichotic tonal stimuli: Some physiological mechanisms of sound localization. *J. Neurophysiol.*, *32*, 613–636.

Graham, B. P., & Dutia, M. B. (2001). Cellular basis of vestibular compensation: Analysis and modelling of the role of the commissural inhibitory system. *Exp. Brain Res.*, *137*, 387–396.

Huterer, M., & Cullen, K. E. (2002). Vestibuloocular reflex dynamics during high-frequency and high-acceleration rotations of the head on body in rhesus monkey. *J. Neurophysiol.*, *88*, 13–28.

Johnston, A. R., MacLeod, N. K., & Dutia, M. B. (1994). Ionic conductances contributing to spike repolarization and after-potentials in rat medial vestibular nucleus neurones. *J. Physiol. (Lond.)*, *481*, 61–77.

Knight, B. W. (1972). Dynamics of encoding in a population of neurons. *J. Gen. Physiol.*, *59*, 734–766.

Masuda, N., & Aihara, K. (2003). Duality of rate coding and temporal coding in multilayered feedforward networks. *Neural Computation*, *15*, 103–125.

Masuda, N., Doiron, B., Longtin, A., & Aihara, K. (2005). Coding of temporally varying signals in networks of spiking neurons with global delayed feedback. *Neural Computation*, *17*, 2139–2175.

Minor, L. B., Lasker, D. M., Backous, D. D., & Hullar, T. E. (1999). Horizontal vestibuloocular reflex evoked by high-acceleration rotations in the squirrel monkey. I. Normal responses. *J. Neurophysiol. 82*, 1254–1270.

Ramachandran, R., & Lisberger, S. (2005). Normal performance and expression of learning in the vestibulo-ocular reflex (VOR) at high frequencies. *J. Neurophysiol. 93*, 2028–2038.

Ramachandran, R., & Lisberger, S. (2006). Transformation of vestibular signals into motor commands in the vestibuloocular reflex pathways of monkeys. *J. Neurophysiol. 96,* 1061–1074.

Ris, L., & Godaux, E. (1998). Neuronal activity in the vestibular nuclei after contralateral or bilateral labyrinthectomy in the alert guinea pig. *J. Neurophys.*, *80*, 2352–2367.

Ris, L., Hachemaoui, M., Vibert, N., Godaux, E., Vidal, P. P., & Moore, L. E. (2001). Resonance of spike discharge modulation in neurons of the guinea pig medial vestibular nucleus. *J. Neurophysiol.*, *86,* 703–716.

Sekirnjak, C., & du Lac, S. (2002). Intrinsic firing dynamics of vestibular nucleus neurons. *J. Neurosci.*, *22*, 2083–2095.

Serafin, M., Vidal, P. P., & Muhlethaler, M. (1996). Electrophysiological study of nucleus gigantocellularis neurons in guinea-pig brainstem slices. *Neuroscience*, *73*, 797–805.

Serafin, M., de Waele, C., Khateb, A., Vidal, P. P., & Muhlethaler, M. (1991). Medial vestibular nucleus in the guinea-pig. I. Intrinsic membrane properties in brainstem slices. *Exp. Brain Res.*, *84*, 417–425.

Serafin, M., Vibert, N., de Waele, C., Vidal, P. P., & Muhlethaler, M. (1996). Electrophysiological properties of nucleus prepositus hypoglossi neurons in guinea-pig brainstem slices. *Soc. Neurosci. Abstr., 22,* 263–262.

Straka, H., Vibert, N., Vidal, P. P., Moore, L. E., & Dutia, M. B. (2005). Intrinsic membrane properties of vertebrate vestibular neurons: Function, development and plasticity. *Prog. Neurobiol.*, *76*, 349–392.

van Rossum, M. C. W. (2001). Transient precision of integrate and fire neurons: Effect of background activity and noise. *J. Comput. Neurosc.*, *10*, 303–310.

van Rossum, M. C. W., Turrigiano, G. G., & Nelson, S. B. (2002). Fast propagation of firing rates through layered networks of neurons. *J. Neurosc., 22*, 1956–1966.